Infectious Disease Modelling 2 (2017) 304–322

Contents lists available at ScienceDirect

Infectious Disease Modelling

journal homepage: www.keaipublishing.com/idm

A new epidemic modeling approach: Multi-regions discrete-time model with travel-blocking vicinity optimal control strategy

Omar Zakary*, Mostafa Rachik, Ilias Elmouki

Laboratory of Analysis, Modeling and Simulation (LAMS), Department of Mathematics and Computer Science, Hassan II University of Casablanca, BP 7955, Sidi Othman, Casablanca, Morocco

ARTICLE INFO

Article history:
Received 12 December 2016
Received in revised form 22 May 2017
Accepted 26 June 2017
Available online 30 June 2017

Keywords:
Multi-regions model
SIR epidemic model
Discrete-time model
Optimal control
Vicinity
Travel-blocking

ABSTRACT

First, we devise in this paper, a multi-regions discrete-time model which describes the spatial-temporal spread of an epidemic which starts from one region and enters to regions which are connected with their neighbors by any kind of anthropological movement. We suppose homogeneous Susceptible-Infected-Removed (SIR) populations, and we consider in our simulations, a grid of colored cells, which represents the whole domain affected by the epidemic while each cell can represent a sub-domain or region. Second, in order to minimize the number of infected individuals in one region, we propose an optimal control approach based on a travel-blocking vicinity strategy which aims to control only one cell by restricting movements of infected people coming from all neighboring cells. Thus, we show the influence of the optimal control approach on the controlled cell. We should also note that the cellular modeling approach we propose here, can also describes infection dynamics of regions which are not necessarily attached one to an other, even if no empty space can be viewed between cells. The theoretical method we follow for the characterization of the travel-locking optimal controls, is based on a discrete version of Pontryagin's maximum principle while the numerical approach applied to the multi-points boundary value problems we obtain here, is based on discrete progressive-regressive iterative schemes. We illustrate our modeling and control approaches by giving an example of 100 regions.

1. Introduction

1.1. Main references and description of the problem

Kermack and McKendrick have contributed to the mathematical theory of epidemics by devising in 1927, the Susceptible-Infected-Removed (SIR) model which has represented a main reference for most mathematical modelers in epidemiology (Kermack & McKendrick, 1927). In SIR compartmental systems, and according to the disease transmission mechanism, a host

* Corresponding author.
E-mail address: zakaryma@gmail.com (O. Zakary).
Peer review under responsibility of KeAi Communications Co., Ltd.

http://dx.doi.org/10.1016/j.idm.2017.06.003

population can be Susceptible, Infected, or Removed. Susceptible individuals are those who are healthy and do not carry the epidemic but can contract it from infected hosts. Infected hosts carry the contagion and are able to pass it on to susceptible hosts. Finally, removed hosts are those who are no longer infected and have acquired immunity from future infection.

In 2016, Zakary et al. published their first papers in (Zakary, Rachik, & Elmouki, 2016a, 2016b, 2016c; Zakary, Larrache, Rachik, Elmoukid, 2016) which have concerned new modeling and optimal control approaches applied to multi-regions SIR models in the continuous-time and discrete-time cases. Additionally, in these mentioned references, the authors supposed that all regions are connected, and then, the incidence rate depends on the number of infected people which come from all regions. However, a region is often infected due to the travel of infected people coming only from the neighboring regions, or generally in the case of detached regions, infection occurs when one or more infected individuals come from regions where there is a possibility to travel to the targeted region. Here, we are more interested in the study of infection dynamics in regions which are not necessarily all connected but in the case when there exists a direct mode of transport between them. For instance, in Fig. 1(a), region 5 is connected with all other regions, and that can represent connections case which has been studied in the references above. In the same figure, we can also see that region 1 is connected only with regions 2, 4 and 5, and such cases have motivated us to write this paper in order to present a new epidemic modeling approach which generalizes all possible cases of infection connections between regions.

More clearly, we propose a cellular representation of regions, assembled all together in one grid of cells, and we study the transmission dynamics of the epidemic in these regions with focusing on only one region, to show the impact of infection connections that relate it with other regions via travel. As illustrated in Fig. 1(b), we can see the example of all 9 regions presented in (a), how they can be converted to cells, assembled in one grid which represents a part of the earth as the global domain of interest.

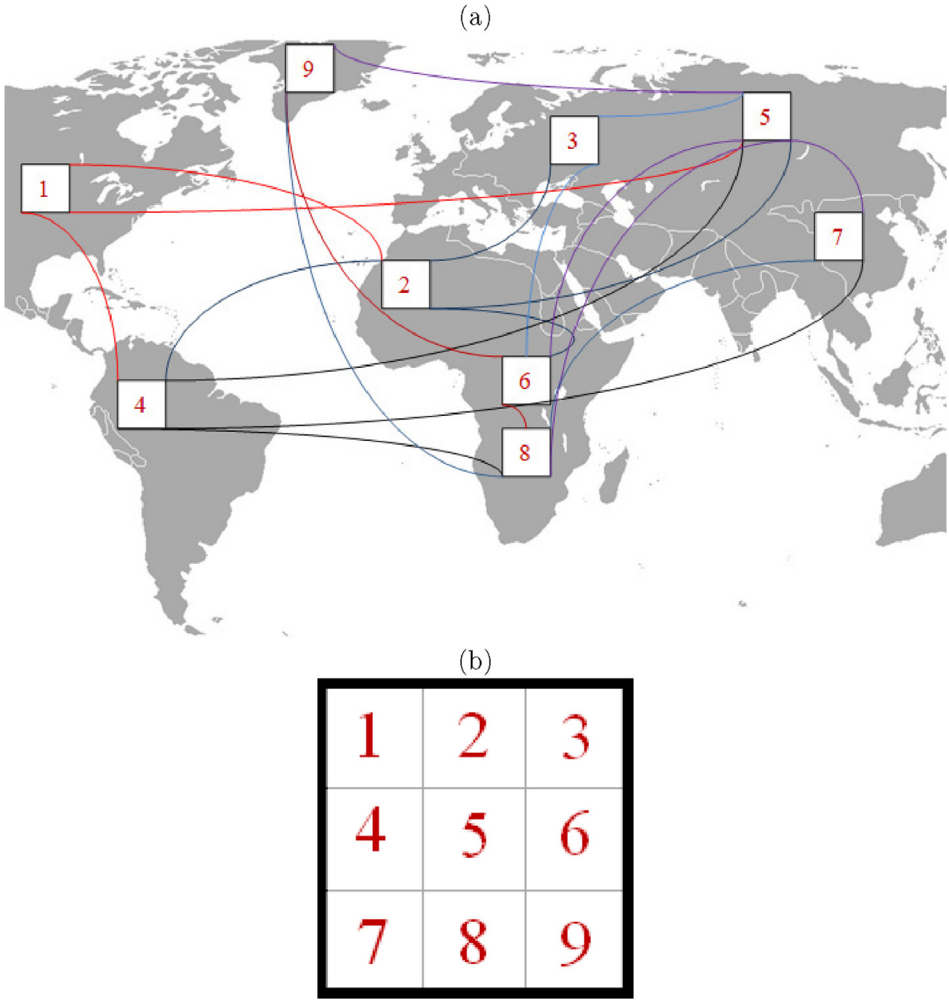

Fig. 1. (a): Infection travel connections between 9 separated geographical regions located at different continents. (b): Assembly of the regions in one grid of 9 numbered cells.

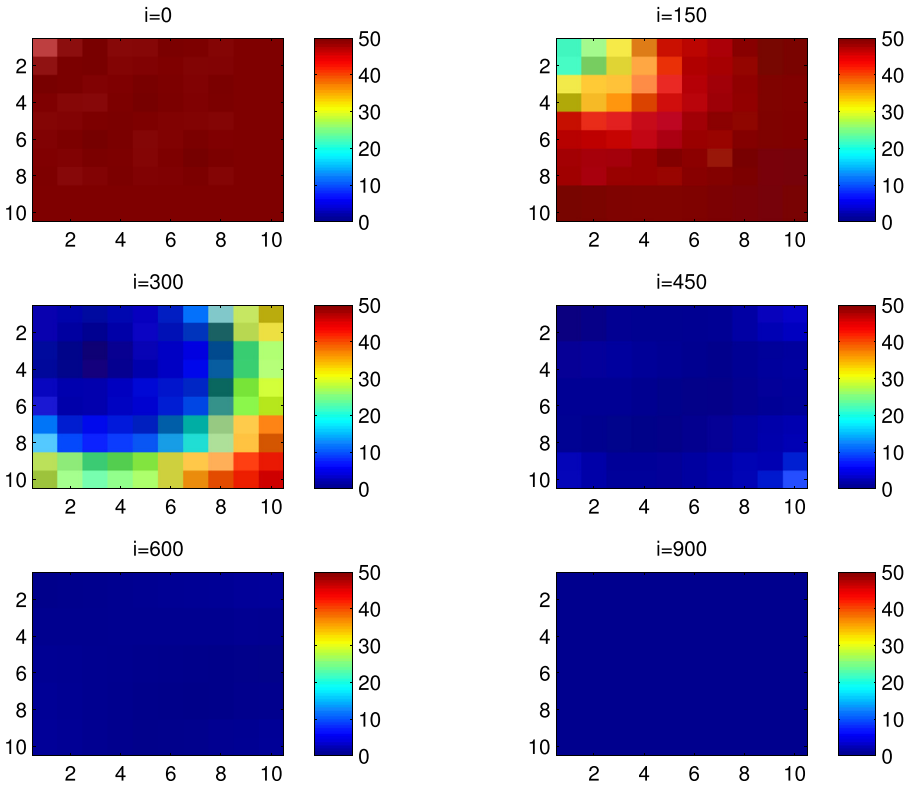

Fig. 2. $S^{C_{pq}}$ behavior in the absence of control. Case when the disease starts from the corner C_{11}.

Based on this new kind of representations, we can discuss the spread of the epidemic and the effectiveness of a control strategy in one region, with the possibility to analyze the SIR dynamics in this region without and with control, and exhibiting the importance of the direct influence between it and its vicinity. As observed in Fig. 1(a) and (b), region 9 is exposed to infection via travel of infected people coming from its vicinity which contains regions 5, 6 and 8, or for same reason, region 8 can directly become highly infected due to connections with regions 4, 5, 6, 7 and 9.

In addition to all those considerations, we note that if Zakary et al. have supposed that all regions are connected by infected travelers to show the influence of SIR dynamics of one region on other regions, the cellular model we propose here, has also the advantage to exhibit this kind of influence even in the absence of direct connections between regions. This can easily understood from the example in Fig. 1 where we can see that region 1 can also be infected by individuals coming from region 7 via region 4. This can be more understood in numerical results we will provide after.

In the following, we provide a brief presentation of the new epidemic modeling and vicinity travel-blocking optimal control approaches.

1.2. The new epidemic model and the vicinity travel-blocking optimal control strategy

The new modeling approach we suggest here, is based on a multi-regions discrete-time epidemic model which describes the spatial-temporal spread of an epidemic which emerges in a global domain of interest Ω represented by a grid of colored cells which are uniform in size. These cells are supposed to be connected by movements of their populations, and they represent sub-domains of Ω or regions, noting that only one of these cells, that is targeted by our control strategy.

In (Zakary et al., 2016a), each region was represented by a sub-domain $(\Omega_j)_{j=1,\dots,p}$ while here, each region or cell is denoted by $(C_{pq})_{p,q=1,\dots,M}$.

For this, we assume that the epidemic can be transmitted and propagated by movements of people, from one spatial cell C_{pq}, to its neighbors or cells belonging to its vicinity. In fact, in a geographical scale relatively small, some infectious diseases such as African Swine Fever (Sánchez-Vizcaíno, Mur, & Martínez-López, 2012), Bovine Viral Diarrhoea virus (Fray, Paton, & Alenius, 2000; Thiaucourt et al., 2000) and Foot-and-Mouth Disease (Grubman & Baxt, 2004), follow that pattern of spread, and C_{pq} can represent a farm, while in a large geographical scale such as in the case of SARS (Afia et al., 2014), HIV/AIDS (Samanta, 2011; Zakary et al., 2016, 2016d), Ebola Virus (Zakary et al., 2016c) and ZIKA Virus (Chunxiao, Tao, & Zhu, 2016), a

cell C_{pq} can represent a city or country. Thus, the multi-cells model with the vicinity optimal control strategy we propose here, can represent good approaches for infection dynamics studies regardless of the area size. In fact, the optimization criteria are chosen here in a way to restrict the movement of people coming from one or more cells and entering other cells. Explicitly, we seek to minimize an objective function associated with C_{pq} and subject to its discrete-time system, with optimal control functions introduced as effectiveness rates of the travel-blocking operations followed between C_{pq} and its neighbors. V_{pq} is he vicinity set, composed by all neighboring cells of C_{pq} and which are denoted by $(C_{rs})_{r=p+k,s=q+k'}$ with $(k,k')\in\{-1,0,1\}^2$ except when $k=k'=0$. Note also as we have mentioned before, these cells are attached just in the grid, but in reality, they are not necessarily joined together as seen in example of Fig. 1(a). For instance, in Fig. 1(b), the vicinity sets associated with regions or cells $C_{11}=\{1\}$, $C_{22}=\{5\}$ and $C_{32}=\{8\}$ are defined by $V_{11}=\{2,4,5\}$, $V_{22}=\{1,2,3,4,6,7,8,9\}$ and $V_{32}=\{4,5,6,7,9\}$ respectively. Thus, the travel-blocking vicinity optimal control approach will show the impact of the optimal blocker control on reducing contacts between susceptible people of the targeted cell C_{pq} and infected people coming from one cell C_{rs} or more cells from V_{pq}.

The paper is organized as follows: Section 2 presents the discrete-time multi-cells epidemic system based a colored cell modeling approach. In Section 3, we announce a theorem of necessary conditions and characterization of the sought optimal controls functions related to the travel-blocking vicinity optimal control approach. Finally, in Section 4, we provide simulations of the numerical results for an example of 100 hypothetical cities when an infection starts from one cell of them and which has 3 neighboring cells (respectively, the case of a cell with 8 neighboring cells is investigated), while aiming to control only one cell with 8 neighboring cells.

2. A discrete-time multi-regions epidemic model

We consider a multi-regions discrete-time epidemic model which describes SIR dynamics within a global domain of interest Ω which in turn is divided to M^2 regions or cells, uniform in size. In other words, $\Omega=\cup_{p,q=1}^{M}C_{pq}$ with C_{pq} denoting a spatial location or region.

We note that $(C_{pq})_{p,q=1,\dots,M}$ could represent a country, a city or town, or a small domain such as neighborhoods, which belong respectively to the global domain of interest Ω which could in turn represent a part of continent or even a whole continent, a part of country or a whole country, etc.

The S-I-R populations associated with a cell C_{pq} are noted by the states $S_i^{C_{pq}}$, $I_i^{C_{pq}}$, and $R_i^{C_{pq}}$, and we note that the transition between them, is probabilistic, with probabilities being determined by the observed characteristics of specific diseases. In addition to the death, there are population movements among these three epidemiological compartments, from time unit i to time $i+1$. We assume that the susceptible individuals are not yet infected but can be infected only through contacts with infected people from V_{pq} (Vicinity set or Neighborhood of a cell C_{pq}), thus, the infection transmission is assumed to occur between individuals present in a given cell C_{pq}, and is given by

$$\sum_{C_{rs}\in V_{pq}}\beta_{rs}I_i^{C_{rs}}S_i^{C_{pq}}$$

where β_{rs} is the constant proportion of adequate contacts between a susceptible from a cell C_{pq} and an infective coming from its neighbor cell $C_{rs}\in V_{pq}$ with $V_{pq}=\{C_{rs}\in\Omega/r=p+k,s=q+k',(k,k')\in\{-1,0,1\}^2\}\setminus C_{pq}$.

SIR dynamics associated with domain or cell C_{pq} are described based on the following multi-cells discrete model For $p,q=1,\dots,M$, we have

$$S_{i+1}^{C_{pq}}=S_i^{C_{pq}}-\beta_{pq}I_i^{C_{pq}}S_i^{C_{pq}}-\sum_{C_{rs}\in V_{pq}}\beta_{rs}I_i^{C_{rs}}S_i^{C_{pq}}-dS_i^{C_{pq}} \tag{1}$$

$$I_{i+1}^{C_{pq}}=I_i^{C_{pq}}+\beta_{pq}I_i^{C_{pq}}S_i^{C_{pq}}+\sum_{C_{rs}\in V_{pq}}\beta_{rs}I_i^{C_{rs}}S_i^{C_{pq}}-(\alpha+\gamma+d)I_i^{C_{pq}} \tag{2}$$

$$R_{i+1}^{C_{pq}}=R_i^{C_{pq}}+\gamma I_i^{C_{pq}}-dR_i^{C_{pq}} \tag{3}$$

$$i=0,\dots,N-1$$

with $S_0^{C_{pq}}\geq 0, I_0^{C_{pq}}\geq 0$ and $R_0^{C_{pq}}\geq 0$ are the given initial conditions.

$d>0$ is the natural death rate while $\alpha>0$ is the death rate due to the infection, $\gamma>0$ denotes the natural recovery rate from infection. By assuming that is all regions are occupied by homogeneous populations, α, d and γ are considered to be the same for all cells of Ω.

3. A travel-blocking vicinity optimal control approach

The main goal of the travel-blocking vicinity optimal control approach is to restrict movements of infected people coming from the set V_{pq} and aiming to reach the cell C_{pq}. For this, we introduce controls $u^{pqC_{rs}}$ variable which characterizes the effectiveness rate of the travel-blocking strategy which limits contacts between susceptible of the targeted cell C_{pq} and infected individuals from cells C_{rs} which belong to V_{pq}. Then, for a given cell C_{pq} in Ω, the discrete-time system (1)-(2)-(3) becomes

$$S_{i+1}^{C_{pq}} = S_i^{C_{pq}} - \beta_{pq} I_i^{C_{pq}} S_i^{C_{pq}} - \sum_{C_{rs}\in V_{pq}} u_i^{pqC_{rs}} \beta_{rs} I_i^{C_{rs}} S_i^{C_{pq}} - dS_i^{C_{pq}} \tag{4}$$

$$I_{i+1}^{C_{pq}} = I_i^{C_{pq}} + \beta_{pq} I_i^{C_{pq}} S_i^{C_{pq}} + \sum_{C_{rs}\in V_{pq}} u_i^{pqC_{rs}} \beta_{rs} I_i^{C_{rs}} S_i^{C_{pq}} - (\alpha+\gamma+d) I_i^{C_{pq}} \tag{5}$$

$$R_{i+1}^{C_{pq}} = R_i^{C_{pq}} + \gamma I_i^{C_{pq}} - dR_i^{C_{pq}} \tag{6}$$

$i = 0, \ldots, N-1$

Since our goal concerns the minimization of the number of the infected people and the cost of the vicinity optimal control approach, we consider an optimization criterion associated with cell C_{pq} and we define it by the following objective function

$$J_{pq}(u) = A_1 I_N^{C_{pq}} + \sum_{i=0}^{N-1} \left(A_1 I_i^{C_{pq}} + \sum_{C_{rs}\in V_{pq}} \frac{A_{rs}}{2} \left(u_i^{pqC_{rs}}\right)^2 \right) \tag{7}$$

where $A_1 > 0$ and $A_{rs} > 0$ are the constant severity weights associated with the number of infected individuals and controls respectively. We note that here, $u = (u_i^{pqC_{rs}})_{C_{rs}\in V_{pq}, i=1,\ldots,N-1}$, which belongs to the control set U_{pq} defined as

$$U_{pq} = \left\{ u = \left(u_i^{pqC_{rs}}\right)_{C_{rs}\in V_{pq}, i=1,\ldots,N-1} \Big/ u^{min} \le u_i^{pqC_{rs}} \le u^{max}, u^{max} < 1\ u^{min} > 0, \right.$$
$$\left. i = 0, \ldots, N-1, C_{rs} \in V_{pq} \right\} \tag{8}$$

Then, we seek optimal control u^* such that

$$J_{pq}(u^*) = min\left\{ J_{pq}(u) / u \in U_{pq} \right\}$$

The sufficient conditions for the existence of optimal controls in the case of discrete-time epidemic models have been announced in (Dabbs, 2010; Wandi, Hendon, Cathey, Lancaster, & Germick, 2014; Zakary et al., 2016a, 2016b).

As regards to the necessary conditions and the characterization of our discrete optimal control, we use a discrete version of Pontryagin's maximum principle (Sethi & Thompson, 2000, pp. 1–22; Zakary et al., 2016a, 2016b).

For this, we define a Hamiltonian $\mathscr{H}$ associated with the cell C_{pq} by

$$\mathscr{H} = A_1 I_i^{C_{pq}} + \sum_{C_{rs}\in V_{pq}} \frac{A_{rs}}{2} \left(u_i^{pqC_{rs}}\right)^2 + \zeta_{1,i+1}^{C_{pq}} \left[S_i^{C_{pq}} - \beta_{pq} I_i^{C_{pq}} S_i^{C_{pq}} - \sum_{C_{rs}\in V_{pq}} u_i^{pqC_{rs}} \beta_{rs} I_i^{C_{rs}} S_i^{C_{pq}} - dS_i^{C_{pq}} \right] + \zeta_{2,i+1}^{C_{pq}} \left[I_i^{C_{pq}} + \beta_{pq} I_i^{C_{pq}} S_i^{C_{pq}} \right.$$
$$\left. + \sum_{C_{rs}\in V_{pq}} u_i^{pqC_{rs}} \beta_{rs} I_i^{C_{rs}} S_i^{C_{pq}} - (\alpha+\gamma+d) I_i^{C_{pq}} \right] + \zeta_{3,i+1}^{C_{pq}} \left[R_i^{C_{pq}} + \gamma I_i^{C_{pq}} - dR_i^{C_{pq}} \right]$$

$i = 0, \ldots, N-1$ with $\zeta_{k,i}^{C_{pq}}, k = 1, 2, 3$, the adjoint variables associated with $S_i^{C_{pq}}$, $I_i^{C_{pq}}$ and $R_i^{C_{pq}}$ respectively, and defined based on formulations of the following theorem.

Theorem 1. *(Necessary Conditions & Characterization)*

Given optimal controls $u^{pqC_{rs}*}$ and solutions $S^{C_{pq}^*}, I^{C_{pq}^*}$ and $R^{C_{pq}^*}$, there exists $\zeta_{k,i}^{C_{pq}}, i = 0 \ldots N, k = 1, 2, 3$, the adjoint variables satisfying the following equations

$$\begin{aligned}
\Delta\zeta_{1,i}^{C_{pq}} &= -\left[(1-d)\zeta_{1,i+1}^{C_{pq}} + \left(\beta_{pq}I_i^{C_{pq}} + \sum_{C_{rs}\in V_{pq}} u_i^{C_{rs}}\beta_{rs}I_i^{C_{rs}}\right)\left(\zeta_{2,i+1}^{C_{pq}} - \zeta_{1,i+1}^{C_{pq}}\right)\right] \\
\Delta\zeta_{2,i}^{C_{pq}} &= -\left[A_1 + \beta_{pq}S_i^{C_{pq}}\left(\zeta_{2,i+1}^{C_{pq}} - \zeta_{1,i+1}^{C_{pq}}\right) + (1-(\alpha+\gamma+d))\zeta_{2,i+1}^{C_{pq}} + \gamma\zeta_{3,i+1}^{C_{pq}}\right] \\
\Delta\zeta_{3,i}^{C_{pq}} &= -\left[(1-d)\zeta_{3,i+1}^{C_{pq}}\right]
\end{aligned} \tag{9}$$

where $\Delta\zeta_{k,i}^{C_{pq}} = \zeta_{k,i+1}^{C_{pq}} - \zeta_{k,i}^{C_{pq}}, k = 1,2,3$*; the difference operator, with* $\zeta_{1,N}^{C_{pq}} = 0, \zeta_{2,N}^{C_{pq}} = A_1, \zeta_{3,N}^{C_{pq}} = 0$*, being the transversality conditions.*

In addition

$$\begin{aligned}
u_i^{pqC_{rs}^*} &= min\left\{max\left\{u^{min}, \right.\right. \\
&\left.\left.\frac{\left(\zeta_{1,i+1}^{C_{pq}} - \zeta_{2,i+1}^{C_{pq}}\right)\beta_{rs}I_i^{C_{rs}^*}S_i^{C_{pq}^*}}{A_{rs}}\right\}, u^{max}\right\}, \\
i &= 0,\ldots,N-1
\end{aligned} \tag{10}$$

Proof. Using a discrete version of Pontryagin's Maximum Principle in (Sethi & Thompson, 2000, pp. 1–22; Zakary et al., 2016a, 2016b), and setting $S^{C_{pq}} = S^{C_{pq}*}$, $I^{C_{pq}} = I^{C_{pq}*}$, $R^{C_{pq}} = R^{C_{pq}*}$ and $u^{pqC_{rs}} = u^{pqC_{rs}*}$ we obtain the following adjoint equations

$$\begin{aligned}
\Delta\zeta_{1,i}^{C_{pq}} &= -\frac{\partial\mathscr{H}}{\partial S_i^{C_{pq}}} \\
&= -\left[(1-d)\zeta_{1,i+1}^{C_{pq}} + \left(\beta_{pq}I_i^{C_{pq}} + \sum_{C_{rs}\in V_{pq}} u_i^{pqC_{rs}}\beta_{rs}I_i^{C_{rs}}\right)\left(\zeta_{2,i+1}^{C_{pq}} - \zeta_{1,i+1}^{C_{pq}}\right)\right]
\end{aligned}$$

$$\begin{aligned}
\Delta\zeta_{2,i}^{C_{pq}} &= -\frac{\partial\mathscr{H}}{\partial I_i^{C_{pq}}} \\
&= -\left[A_1 + \beta_{pq}S_i^{C_{pq}}\left(\zeta_{2,i+1}^{C_{pq}} - \zeta_{1,i+1}^{C_{pq}}\right) + (1-(\alpha+\gamma+d))\zeta_{2,i+1}^{C_{pq}} + \gamma\zeta_{3,i+1}^{C_{pq}}\right]
\end{aligned}$$

$$\begin{aligned}
\Delta\zeta_{3,i}^{C_{pq}} &= -\frac{\partial\mathscr{H}}{\partial R_i^{C_{pq}}} \\
&= -\left[(1-d)\zeta_{3,i+1}^{C_{pq}}\right]
\end{aligned}$$

with $\zeta_{1,N}^{C_{pq}} = 0, \zeta_{2,N}^{C_{pq}} = A_1, \zeta_{3,N}^{C_{pq}} = 0$; the transversality conditions.

In order to obtain the optimality condition, we calculate the derivative of H with respect to $u_i^{pqC_{rs}}$, and we set it equal to zero

$$\frac{\partial\mathscr{H}}{\partial u_i^{pqC_{rs}}} = A_{rs}u_i^{pqC_{rs}} - \zeta_{1,i+1}^{C_{pq}}\beta_{rs}I_i^{C_{rs}}S_i^{C_{pq}} + \zeta_{2,i+1}^{C_{pq}}\beta_{rs}I_i^{C_{rs}}S_i^{C_{pq}} = 0$$

Then, we obtain

$$u_i^{pqC_{rs}} = \frac{\left(\zeta_{1,i+1}^{C_{pq}} - \zeta_{2,i+1}^{Cpq}\right)\beta_{rs}I_i^{C_{rs}}S_i^{C_{pq}}}{A_{rs}}$$

By the bounds in U_{pq}, we finally obtain the characterization of the optimal controls $u_i^{pqC_{rs}^*}$ as

Table 1
Parameters values of α, β, γ and d associated with a cell $\boldsymbol{C_{pq}}, \boldsymbol{p}, \boldsymbol{q} = \boldsymbol{1}, \ldots, \boldsymbol{M}$, and which utilized for the resolution of all multi-regions discrete-time systems (1)-(2)-(3) and (4)-(5)-(6), and then leading to simulations obtained from Figs. 2 to Fig. 17, with the initial conditions $\boldsymbol{S_0^{C_{pq}}}, \boldsymbol{I_0^{C_{pq}}}$ and $\boldsymbol{R_0^{C_{pq}}}$ associated with any cell $\boldsymbol{C_{pq}}$ of Ω.

$S_0^{C_{pq}}$	$I_0^{C_{pq}}$	$R_0^{C_{pq}}$	α	β	γ	d
50	0	0	0.002	0.0001	0.003	0.0001

$$u_i^{pqC_{rs}^*} = min\left\{ max\left\{ u^{min}, \frac{\left(\zeta_{1,i+1}^{C_{pq}} - \zeta_{2,i+1}^{C_{pq}}\right)\beta_{rs} I_i^{C_{rs}^*} S_i^{C_{pq}^*}}{A_{rs}} \right\}, u^{max} \right\} \tag{11}$$
$$i = 0, \ldots, N-1, , C_{rs} \in V_{pq}$$

4. Numerical results and discussions

4.1. Brief presentation

In this section, we provide numerical simulations to demonstrate our theoretical results in the case when the studied domain Ω , represent the assembly of M^2 regions or cells (cities, towns, …). A code is written and compiled in MATLAB using data cited in Table 1. The optimality systems are solved using an iterative method where at instant i, the states $S_i^{C_{pq}}$, $I_i^{C_{pq}}$, and $R_i^{C_{pq}}$ with an initial guess, are obtained based on a progressive scheme in time, and their adjoint variables $\zeta_{l,i}^{C_{pq}}$, $l = 1, 2, 3$ are obtained based on a regressive scheme in time because of the transversality conditions. Afterwards, we update the optimal controls values (10) using the values of state and costate variables obtained in the previous steps. Finally, we execute the previous steps till a tolerance criterion is reached. In order to show the importance of our work, and without loss of generality, we consider here that $M = 10$ and then we present our numerical simulations in a 10×10 grid and which represents the global domain of interest Ω.

At the initial instant $i = 0$, susceptible people are homogeneously distributed with 50 individuals in each cell except at the upper left corner cell C_{11}, where we introduce 10 infected individuals and 40 susceptible ones, and with similar values, we study the case when the epidemic starts from the cell C_{65} which is near to the center of Ω.

In all of the figures below, the redder part of the colorbars contains larger numbers of individuals while the bluer part contains the smaller numbers.

In the following, we discuss with more details, the cellular simulations we obtain, in the case when there is yet no control.

4.2. Cellular simulations without controls

In this section, Figs. 2–7 depict dynamics of the susceptible population in the case when there is yet no control strategy, followed for the prevention of the epidemic, and we note that in all these figures presented here, simulations give us an idea about the spread of the disease in two different cases:

- When the epidemic starts in a cell C_{pq} with $p = 1, q = 1$ (upper left corner cell). It represents the case when the vicinity set V_{pq} associated with the source cell of infection, contains 3 cells).
- When the epidemic starts from a cell C_{pq} with $p = 6, q = 5$, located in the vicinity of the target cell we aim to control.

For instance, in Fig. 2, if we suppose there are 40 susceptible people in cell C_{11} located at the upper left corner of Ω, and 50 in each other cell, we can see that at instant $i = 150$, the number $S^{C_{11}}$ becomes less important and takes a value close/or equal to 20, while $S^{C_{pq}}$ in cells of V_{11} take values close/or equal to 30, and as we move away from $V_{11} = \{C_{12}, C_{21}, C_{22}\}$, $S^{C_{pq}}$ remains important. At instant $i = 300$, we can observe that in most of cells, $S^{C_{pq}}$ becomes less important, taking values between 0 and 10 while in other cells, it takes values between 20 and 40 except $S^{C_{1010}}$ which conserves its value in 50 since it is located far away from the source of infection. At instant $i = 450$, $S^{C_{pq}}$ becomes zero except at the corners and in most cells at the borders of Ω because these cells have vicinity sets smaller than other cells. Finally at last instants, $S^{C_{pq}}$ converge to zero in all cells. As regards to Fig. 3, when we consider $S^{C_{65}} = 40$ which is located near the center of Ω, and 50 susceptible people in each other cell, it is observed that the situation is more severe, because the disease reaches the corners and borders faster than the case of Fig. 2 As we can see at instant $i = 300$, $S^{C_{pq}}$ takes values less important in most cells except at the corners and borders since their vicinity sets contain only 3 to 5 cells respectively, but it is a result we have reached until instant $i = 450$ in Fig. 2.

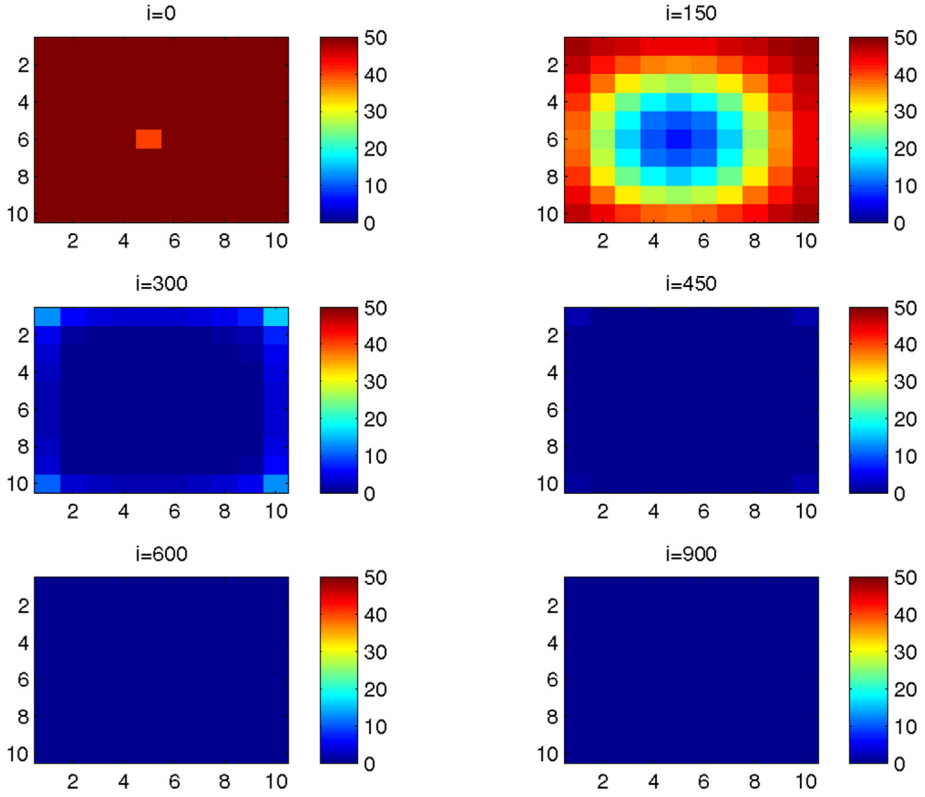

Fig. 3. $S^{C_{pq}}$ behavior in the absence of control. Case when the Disease starts near the center of Ω, exactly at C_{65}.

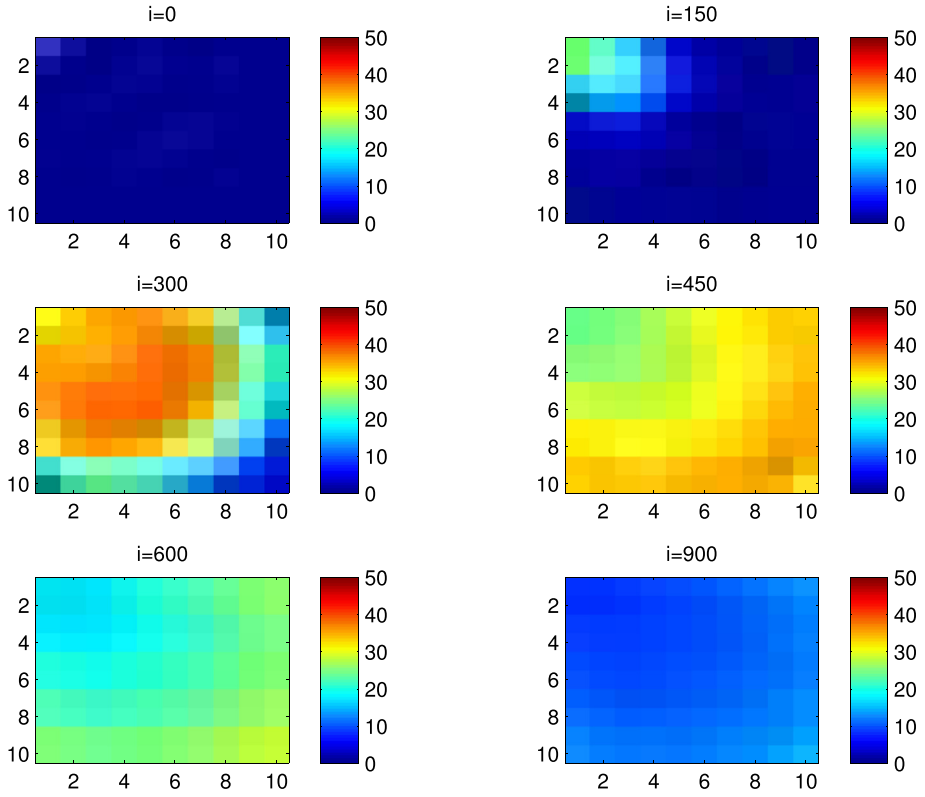

Fig. 4. $I^{C_{pq}}$ behavior in the absence of control. Case when the disease starts from the corner C_{11}.

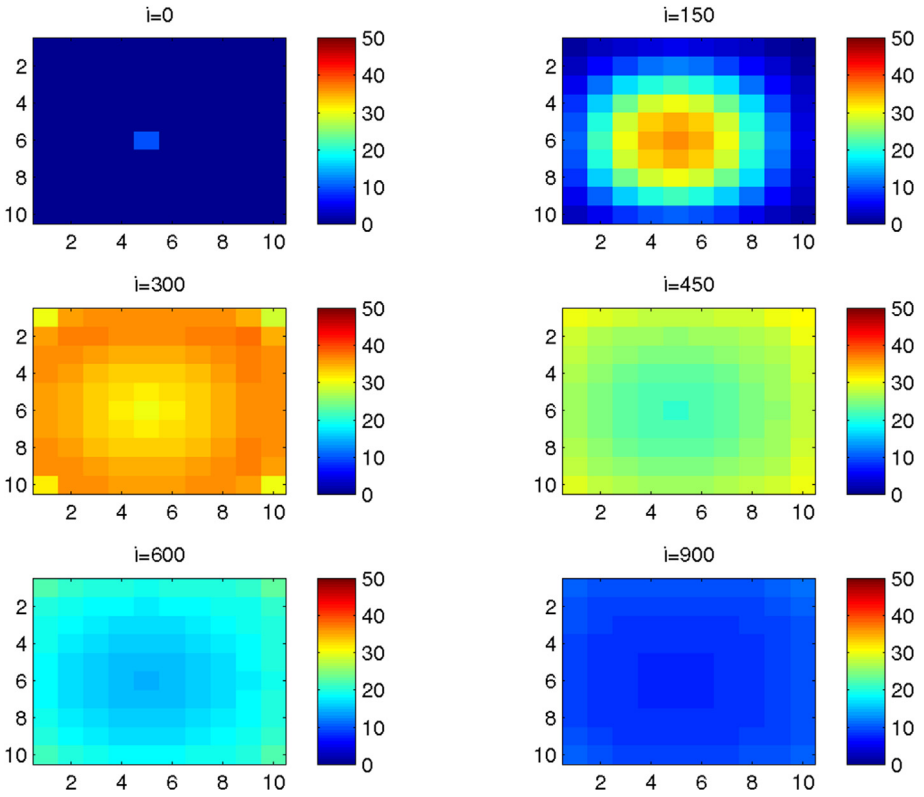

Fig. 5. $I^{C_{pq}}$ behavior in the absence of control. Case when the Disease starts near the center of Ω, exactly at C_{65}.

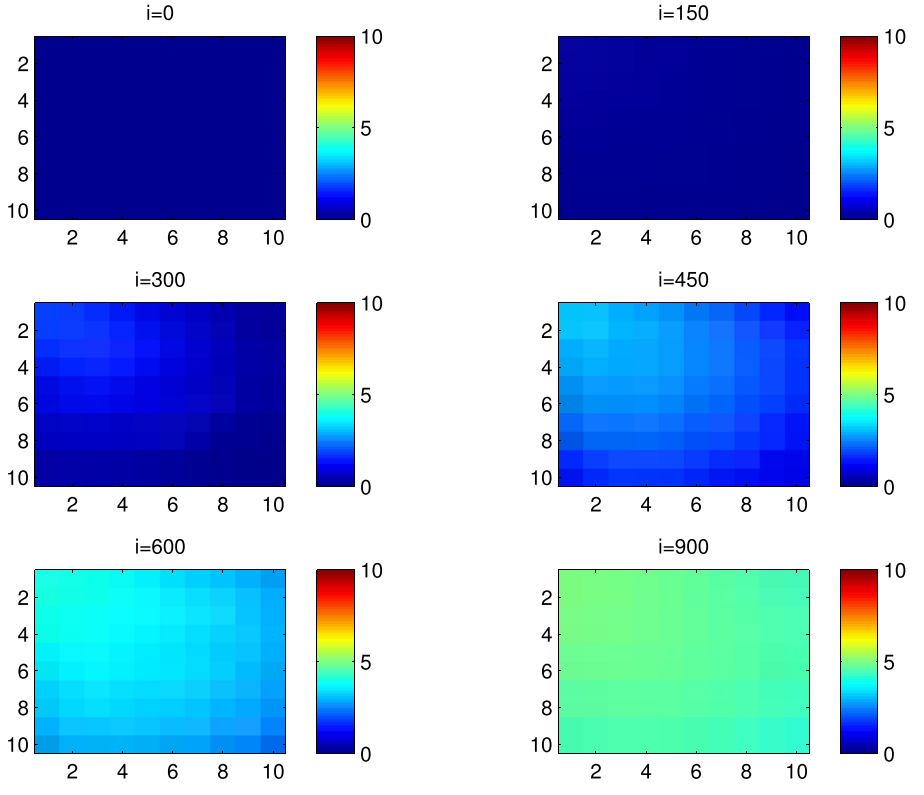

Fig. 6. $R^{C_{pq}}$ behavior in the absence of control. Case when the disease starts from the corner C_{11}.

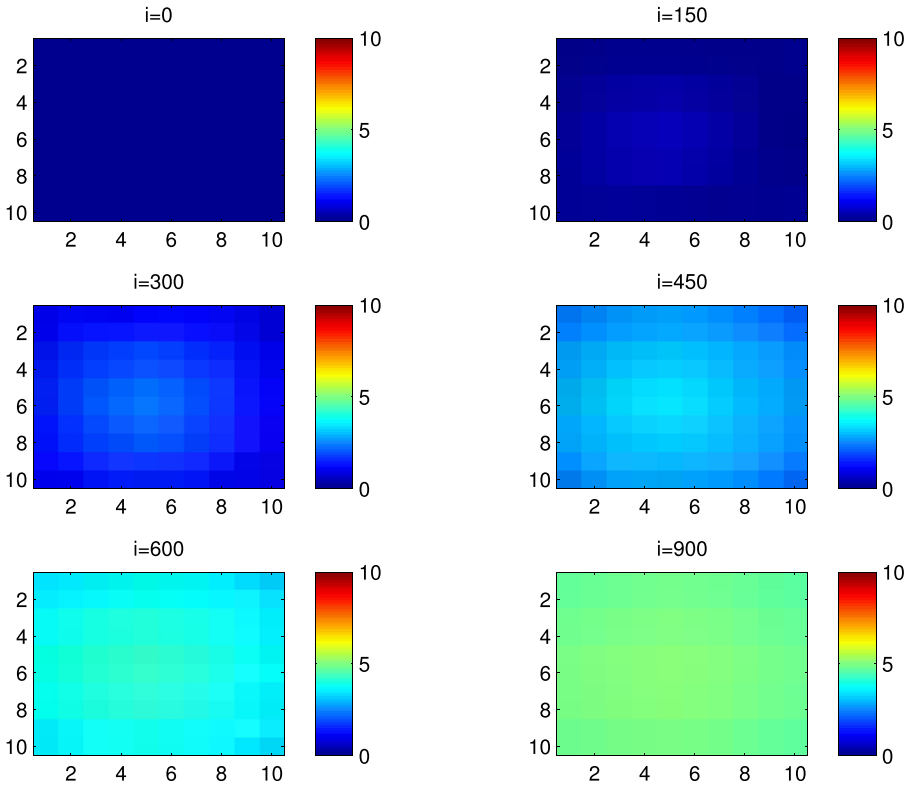

Fig. 7. $R^{C_{pq}}$ behavior in the absence of control. Case when the Disease starts near the center of Ω, exactly at C_{65}.

Figs. 4 and 5 illustrate the rapid propagation of the infection when the disease starts from cell C_{11}, and when it starts from the center of Ω respectively. In Fig. 4, if we suppose there are 10 infected people in cell C_{11}, and no infection in all other cells, we observe that at instant $i = 150$, the number $I^{C_{11}}$ increases to bigger values close/or equal to 30 in C_{22}, while $I^{C_{pq}}$ in cells of V_{11} take values close/or equal to 20, and as we move away from V_{11}, $I^{C_{pq}}$ remains less important. At instant $i = 300$, we can see that in most of cells, $I^{C_{pq}}$ becomes more important, taking values between 30 and 35 in cells which are close to cells with 8 neighboring cells, while in few other cells, it takes values between 0 and 20. From these numerical results, we can deduce that once the infection arrives to the center or to the cells with 8 cells in their vicinity sets, the infection becomes more important compared to the case of the previous instant. At instant $i = 450$, $I^{C_{pq}}$ takes values close/or equal to 20 in the cell from where the epidemic has started, and 25 in V_{11} and near to it, and as we move away towards the center and further regions, infection is important with the presence of more than 30 infected individuals in each cell except the ones in the 3 opposite corners even at instant $i = 600$. In fact, at the center of Ω, the number of infected people which has increased to 35 at the previous instant, has been reduced, because once a cell becomes highly infected, it loses an important number of individuals which die or recover naturally after. All cells C_{pq} become highly infected and the number $I^{C_{pq}}$ becomes less and less important at further instants, noting that at $i = 900$, a large number of infected individuals, has decreased because many $I^{C_{pq}}$ have died or moved to the removed compartment. In Fig. 5, when we consider infection starting from near the center of Ω by considering now that $I^{C_{65}} = 10$, and no infected people in other cells, the disease spreads towards the corners and borders faster than the first case in Fig. 4. At instant $i = 150$, the number of infected people has increased in V_{65}, and as more we move away to the corners and borders, infection is still low. At instant $i = 300$, $I^{C_{pq}}$ takes values more important in most cells, close/or equal to 35, except at the corners and center where $I^{C_{pq}}$ is close/or equal to 30, which is a result we can reach until instant $i = 450$ in Fig. 4, noting that $I^{C_{65}}$ and $I^{C_{pq}}$ in $V^{C_{65}}$ have reduced due to death or natural recovery from the disease, while the infection has remained important in cells which are near to the corners and borders since the infection has just arrived. The corner cells at instant $i = 450$ conserve their number of infected individuals while cells at the borders of Ω and the ones which are close to the center, lose more people due to the number of dead or recovered people which increases more and more at further instants, leading $I^{C_{65}}$ to decrease towards 13 and 8 at $i = 600$ and $i = 900$ respectively.

We note that in the following figure, the scale of the colorbars, does not exceed 10 individuals since we can not reach larger number of removed people when we focus only on targeting infected people which come from C_{11}. As we can observe in Fig. 6, when we have supposed there are 40 susceptible people in cell C_{11}, and 50 in each other cell, we can see here that

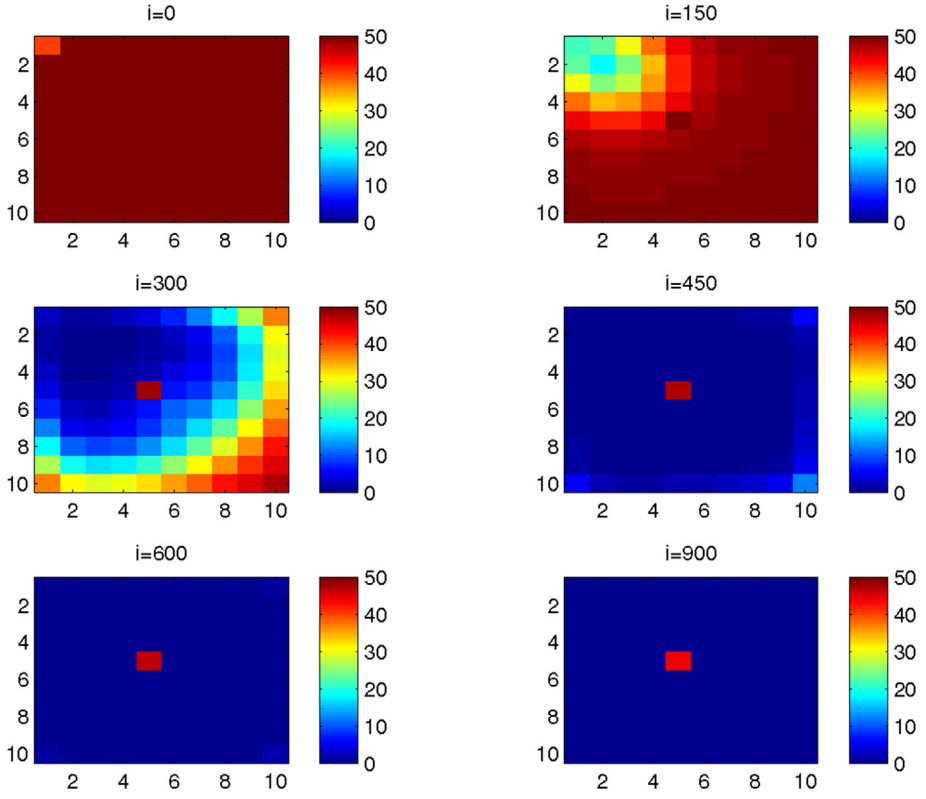

Fig. 8. $S^{C_{pq}}$ behavior in the presence of optimal controls (10). Case when the disease starts from the corner C_{11}.

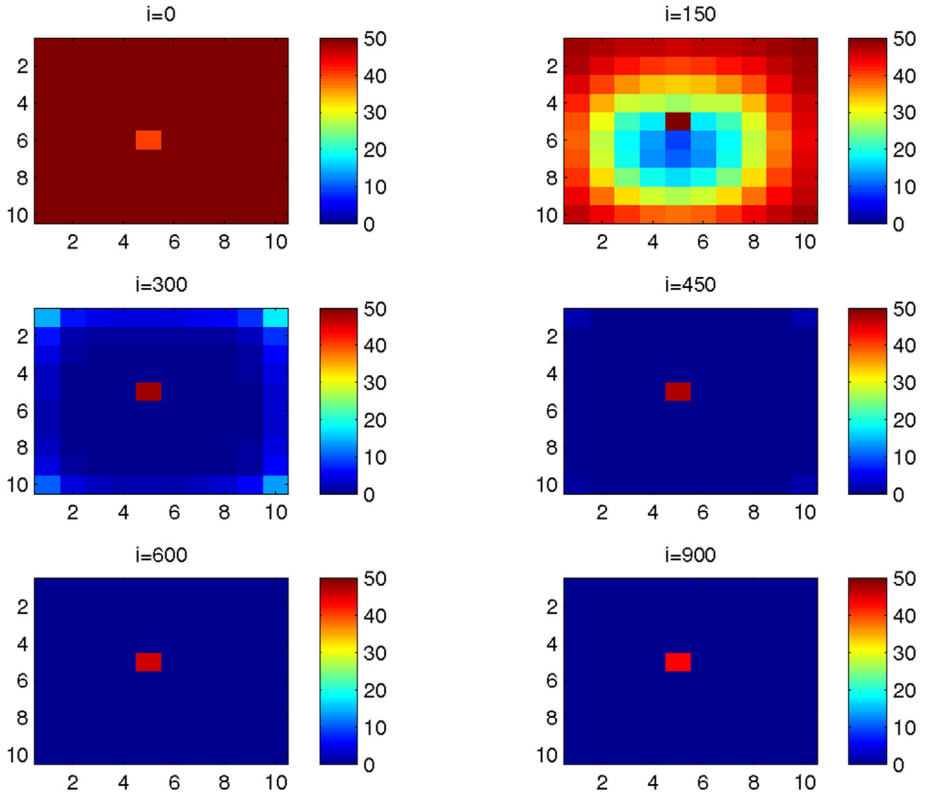

Fig. 9. $S^{C_{pq}}$ behavior in the presence of optimal controls (10). Case when the disease starts near the center of Ω, exactly at C_{65}.

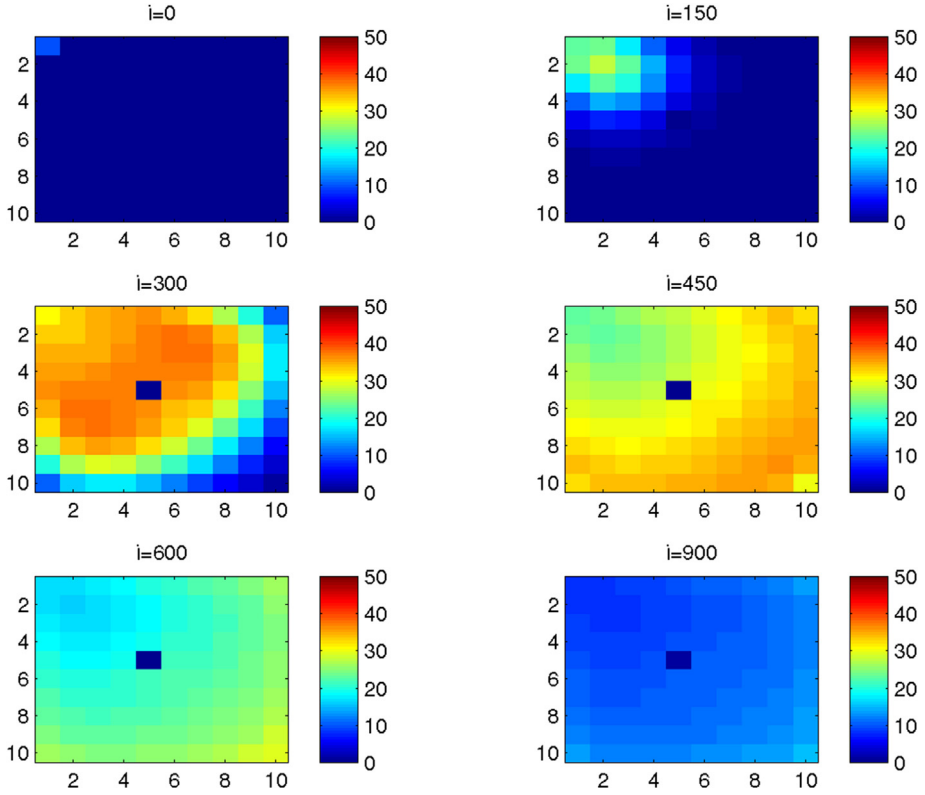

Fig. 10. $I^{C_{pq}}$ behavior in the presence of optimal controls (10). Case when the disease starts from the corner C_{11}.

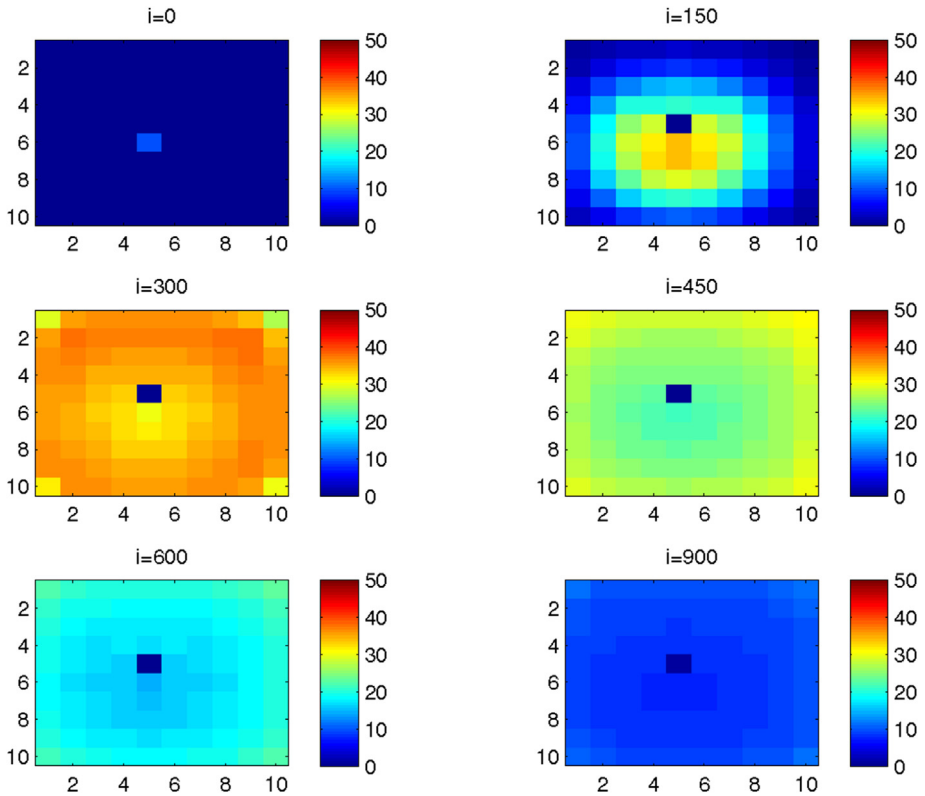

Fig. 11. $I^{C_{pq}}$ behavior in the presence of optimal controls (10). Case when the disease starts near the center of Ω, exactly at C_{65}.

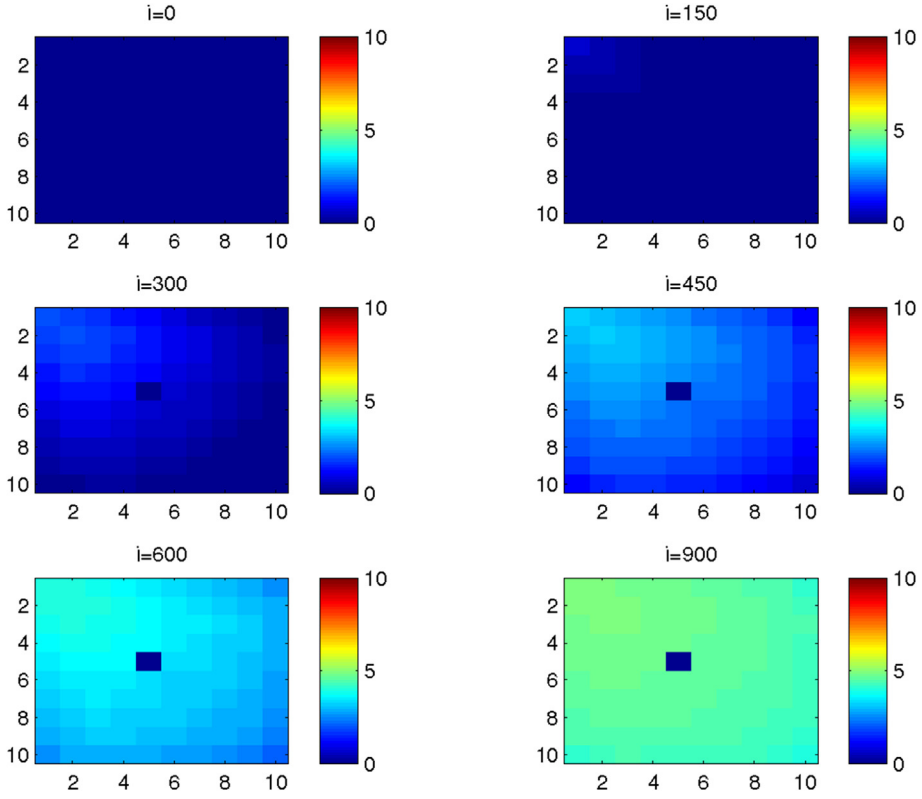

Fig. 12. $S^{C_{pq}}$ behavior in the presence of optimal controls (10). Case when the disease starts from the corner C_{11}.

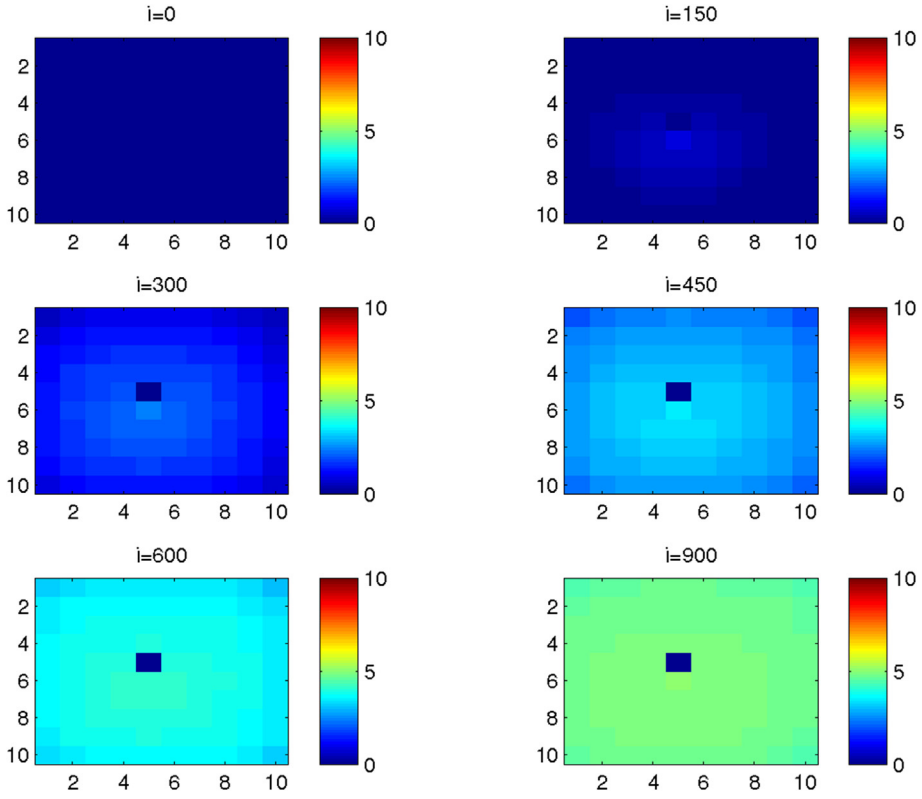

Fig. 13. $S^{C_{pq}}$ behavior in the presence of optimal controls characterized in (10). Case when the disease starts near the center of Ω, exactly at C_{65}.

simultaneously, at instant $i = 150$, the number $R^{C_{11}}$ and $R^{C_{pq}}$ in cells of V_{11} are close/or equal to only 1 or two removed people, and as we move away from V_{11}, $R^{C_{pq}}$ becomes zero. Similarly, at instant $i = 300$, the number $R^{C_{pq}}$ is not zero and takes values between 1 and 3, except for distant cells where it remains zero. At instant $i = 450$, $R^{C_{pq}}$ takes values between 3 and 5 except at the opposite 3 corners and some cells at the borders where it does not exceed 2 removed people. Finally, at further instants $R^{C_{pq}}$ converge to 5 in most cells at $i = 600$ and in all cells at $i = 900$ since as more we go forward in time, some people acquire immune responses that help them to cure naturally from the disease. As regards to Fig. 7, when we consider $S^{C_{65}} = 40$ located near the center of Ω, we can see that, results at instant $i = 600$ when the disease has started from the upper left corner of Ω, are at most the same as results obtained at $i = 450$ when the disease has started near the center of Ω since at instant $i = 300$, $R^{C_{pq}}$ have already begun to increase from the center because some infected people have disappeared as seen in previous figure. As regards to further numerical simulations, we can observe that the number of the removed people increases to 5 at the center at $i = 450$ until it reaches the same value in all cells of Ω except the corners at $i = 600$, and it becomes more and more important at further instants reaching 5 removed people at the corners and 6 in each other cell at $i = 900$.

In the following, we discuss the cellular simulations we obtain, in the case when the optimal controls (10) are introduced.

4.3. Cellular simulations with controls

Figs. 8–13 depict dynamics of the SIR populations when the travel-blocking vicinity optimal control strategy is followed.

In order to show the importance of the optimal control approach suggested in this paper, we take the example of a cell which has 8 neighboring cells, and as done in the previous part, we investigate also here, the results obtained when the disease starts from a corner and when it starts near or attached to the center. As an example, we suppose that the cell we aim to control is C_{55}, and we present simulations when the epidemic is more important at the corner cell C_{11}, and when the epidemic is more important in the cell C_{65} which is attached or directly connected to C_{55}.

In Fig. 8, as supposed also above, there are 40 susceptible people in cell C_{11}, and 50 in each other cell. We can see that at instant $i = 150$, the numbers $S^{C_{11}}$ and $S^{C_{pq}}$ are at most the same as in the case when there was no control strategy. At instant $i = 300$, we can observe that in most of cells, $S^{C_{pq}}$ becomes less important, taking values between 0 and 10 in cells that are close to V_{11}, while in other cells, and as more we move away from V_{11}, it takes values between 20 and 40. However, the controlled cell C_{55} contains 45 susceptible people. In fact, even at instant $i = 150$, the number of susceptible people in the controlled cell conserved its value in 50, which is not also exactly the same as in the case when there was yet no control strategy since in Fig. 2, $S^{C_{pq}}$ has decreased more significantly. Thus, we can deduce that the travel-blocking vicinity optimal control strategy has proved its effectiveness earlier in time. At instants $i = 450, 600$ and $i = 900$, $S^{C_{pq}}$ is also the same as done before but fortunately again, we reach our goal in keeping the number $S^{C_{55}}$ close to its initial value despite some small decrease. Thus, this demonstrates that most of movements of infected people coming from the vicinity set $V^{C_{55}}$, have been restricted in final times. As regards to Fig. 9, when we consider $S^{C_{65}} = 40$ which represents the number of susceptible people which are present in cell C_{65} located near the center of Ω and exactly in the vicinity of the target cell C_{55} which we aims to control since we have $C_{65} \in V_{56} = \{C_{45}, C_{47}, C_{54}, C_{66}, C_{46}, C_{57}, C_{67}, C_{47}\}$, and we consider 50 susceptible people in each other cell. We can observe at instant $i = 300$, that $S^{C_{pq}}$ takes values less important in most cells except at the corners and borders since the number of cells in their vicinity sets is small, but it is a result we have reached until instant $i = 450$ in Fig. 8, and we can see more clearly that the cell $S^{C_{55}}$ has decreased to only 45 since even in the previous instant $i = 150$, $S^{C_{55}}$ has not changed also and conserved its value in 50. At that instant, and as shown also in the previous case, the corner cells contain about 20 susceptible while in cells in the borders, $S^{C_{pq}}$ take values between 10 and 15, and 0 in some cells near to the corners. Finally, as we move forward in time, it is observed that the targeted cell C_{55} has not changed significantly the number of its susceptible people at all, but loses only about 10 people due to uncontrolled infection.

In Fig. 10, we can see more the analogy between the number of susceptible people $S^{C_{11}}$ and $S^{C_{65}}$ and infected ones $I^{C_{11}}$ and $I^{C_{65}}$. In fact, when the disease starts from cell C_{11}, as supposed in the section above, there are 10 infected people in cell C_{11}, and no infected in each other cell, and we can deduce that at instant $i = 150$, the numbers $I^{C_{11}}$ and $I^{C_{pq}}$ are at most the same, as shown in the absence of controls. At instant $i = 300$, we can see that in most of cells, $I^{C_{pq}}$ is similar to the case in Fig. 3, and it is also more important, taking values between 20 and 30 while in other cells, it takes values between 0 and 10 as shown in the previous subsection. However, the controlled cell C_{55} is still not really infected and contains only about one infected individual. At instant $i = 450$, $I^{C_{pq}}$ takes values around 20 in neighboring cells which belong to V_{11}, and about 30 in other cells except at the 3 opposite corners and borders of Ω. At instant $i = 600$, most cells C_{pq} begin to lose some infected individuals due to natural recovery and the number $I^{C_{pq}}$ becomes less and less important at further instants while $I^{C_{55}}$ does not exceed 2 infected individuals. In Fig. 11, and as done in case without controls, we can also observe that when we consider infection starting from near the center of Ω by supposing $I^{C_{65}} = 10$ with no infected people in each other cell, the disease spreads towards the corners and borders faster than the first case in Fig. 10. For instance, at instant $i = 150$, the number of infected people has increased in V_{55} and V_{65}, and as more we move away to the corners and borders, infection is still low. At instant $i = 300$, $I^{C_{pq}}$ takes values more important in most cells except at the corners, which is a result we can reach until instant $i = 600$ in Fig. 10, noting that $I^{C_{55}}$, and $I^{C_{pq}}$ in $V^{C_{55}}$ has reduced due to death or natural recovery from the disease, while the

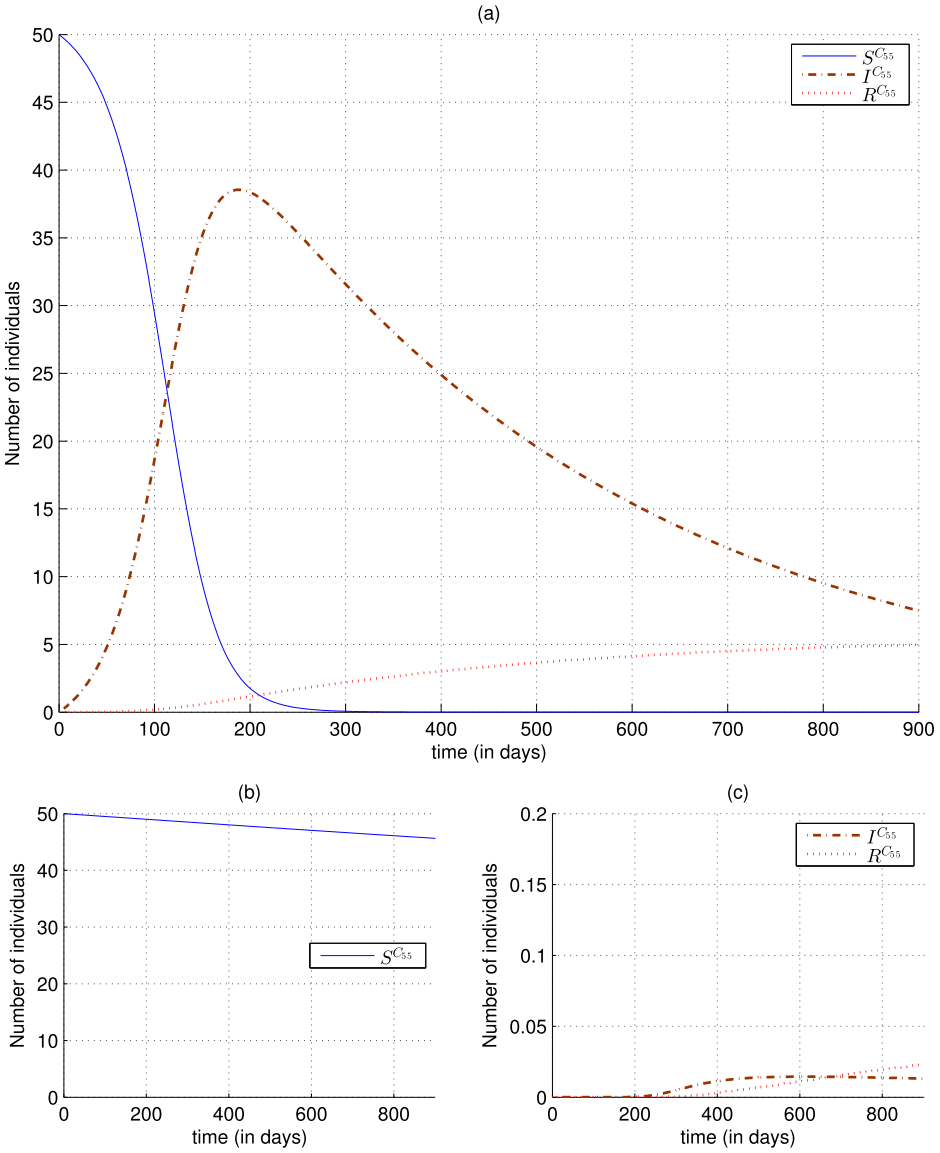

Fig. 14. (a): $S^{C_{55}}$, $I^{C_{55}}$ and $R^{C_{55}}$ associated with the targeted cell C_{55} without controls. (b) & (c): $S^{C_{55}}$, $I^{C_{55}}$ and $R^{C_{55}}$ associated with the controlled cell C_{55} in the presence of optimal controls (10) with $p = q = 5$.

infection becomes important in cells which are near to the corners and borders. The corner cells at instant $i = 450$ conserve their number of infected individuals while some cells at the borders of Ω and the ones which are close to the center, lose more people due to the number of dead or removed people which increases more and more at further instants as observed in $i = 600$ and $i = 900$ where C_{55} does not exceed 2 infected individuals.

In Fig. 12, when we suppose there are 40 susceptible people in cell C_{11}, and 50 others in each other cell, we can see that simultaneously, at instant $i = 150$, the number $R^{C_{11}}$ takes a value close/or equal to 5, while $R^{C_{pq}}$ in cells of V_{11} are zero, and as we move away from V_{11}, $R^{C_{pq}}$ is still zero. Similarly, at instant $i = 300$, the number $R^{C_{pq}}$ is zero at the 3 opposite corners and borders of Ω while it takes values between 1 and 3 in other cells, but $R^{C_{55}}$ is still very close to zero since very few people who have been infected there. At instant $i = 450$, $R^{C_{pq}}$ takes values between 2 and 4 except at the corners and borders while C_{55} is still not containing more than 1 or 2 people in its removed compartment. Finally at last instants, $R^{C_{pq}}$ converge to 4 at $i = 600$ in all cells except in C_{55}, and between 5 or 6 in all cells at $i = 900$ and a number of individuals close to zero in C_{55} since not many individuals have been infected to move to the removed compartment. As regards to Fig. 13, when we consider $S^{C_{65}} = 40$, we can see that at instant $i = 600$, in all cells C_{pq}, the number of the removed people increases to 4 in the corner cells, and 5 in

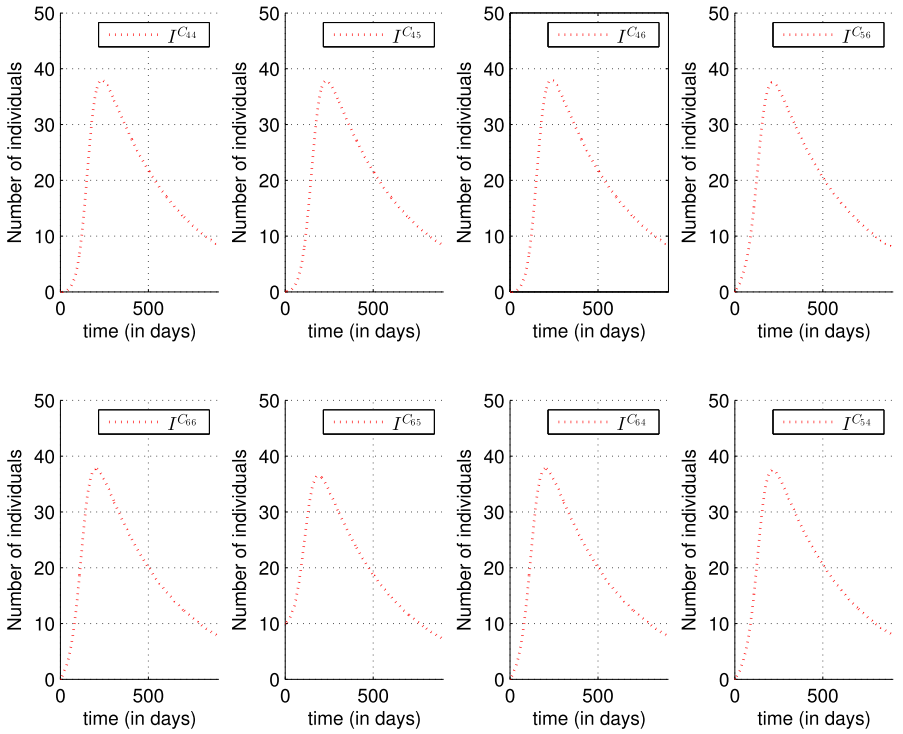

Fig. 15. Shape of $I^{C_{rs}}$ in the presence of optimal controls (10) when $p = q = 5$, $r = 5 + k, s = 5 + k', (k, k') \in \{-1, 0, 1\}^2$ with $k \neq k'$ *when* $k = 0$ *or* $k' = 0$.

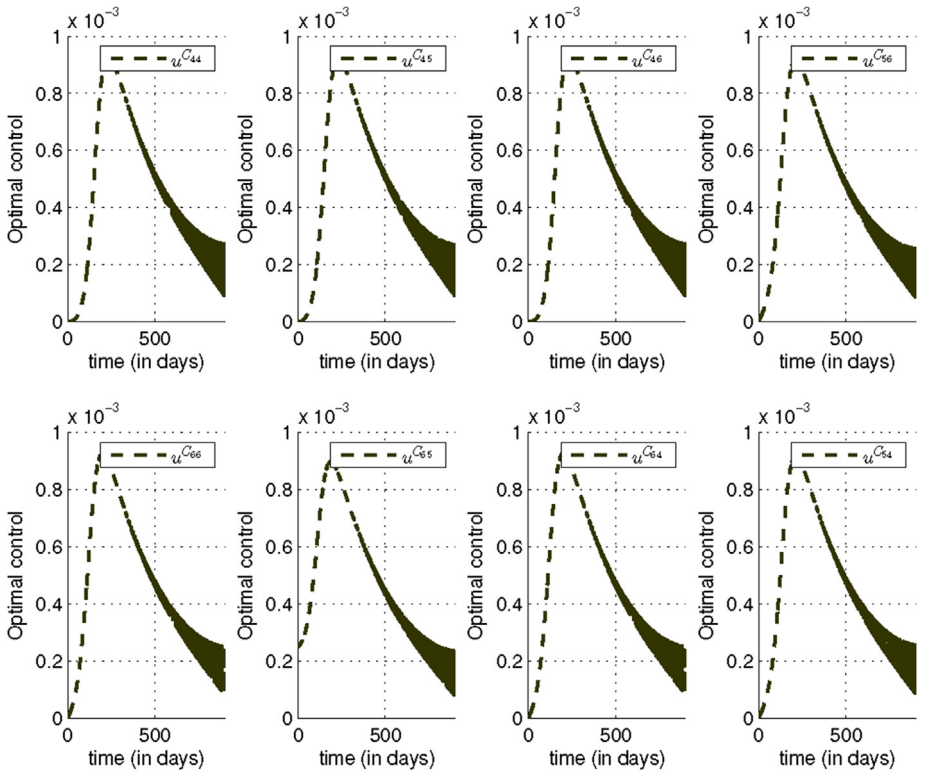

Fig. 16. Optimal controls $u^{55C_{rs}}, r = 5 + k, s = 5 + k', (k, k') \in \{-1, 0, 1\}^2$ with $k \neq k'$ *when* $k = 0$ *or* $k' = 0$.

most cells of Ω, and to 6 when we go forward in time as we can observe at instant $i = 900$ while $R^{C_{55}}$ has not changed significantly.

4.4. Discussions

Fig. 14(a) illustrates the shapes of the functions $S^{C_{55}}$, $I^{C_{55}}$ and $R^{C_{55}}$ alone, without the cellular representations of the other cells. From this figure, we can see that in the case when there was yet no control strategy followed in the vicinity of the targeted cell C_{55}, that as the number of susceptible people tends towards 0, the number of removed people increases but does not exceeded 5 individuals since there are more than 7 individuals which have not acquired sufficient natural immunity to cure from the disease. In the opposite side, when we apply the travel-blocking vicinity approach to the middle cell C_{55}, we can deduce from Fig. 14(b), that the number of susceptible people in C_{55}, has not decreased significantly since the difference between the initial and final conditions is only about 5 individuals. This could be explained by the fact that those few individuals have disappeared because natural death only, since there was no real infection in C_{55}, which could seriously affect the other 45 susceptible people. In fact, as seen in Fig. 14(c), the infection is insignificant, not exceeding the value 0.0125, which is the same to say no individual has been really infected, while in the last compartment, we can also observe that the number of the removed people is not important since a recovery requires infection first. Thus, we can finally deduce that we have reached an important restriction of the movements of infected populations coming from the vicinity set V_{55}. In Figs. 15 and 16, we can see with more details the values of the infection which has been present in the vicinity set V_{55} and with which optimal controls, it has been prevented.

We can observe from Fig. 15, that the number of infected people in cells which belong to V_{55}, all increase after 250 days, towards 38 individuals, except in the cell C_{65} where $I^{C_{65}}$ increases towards the same value but minus 2 individuals. In fact, the

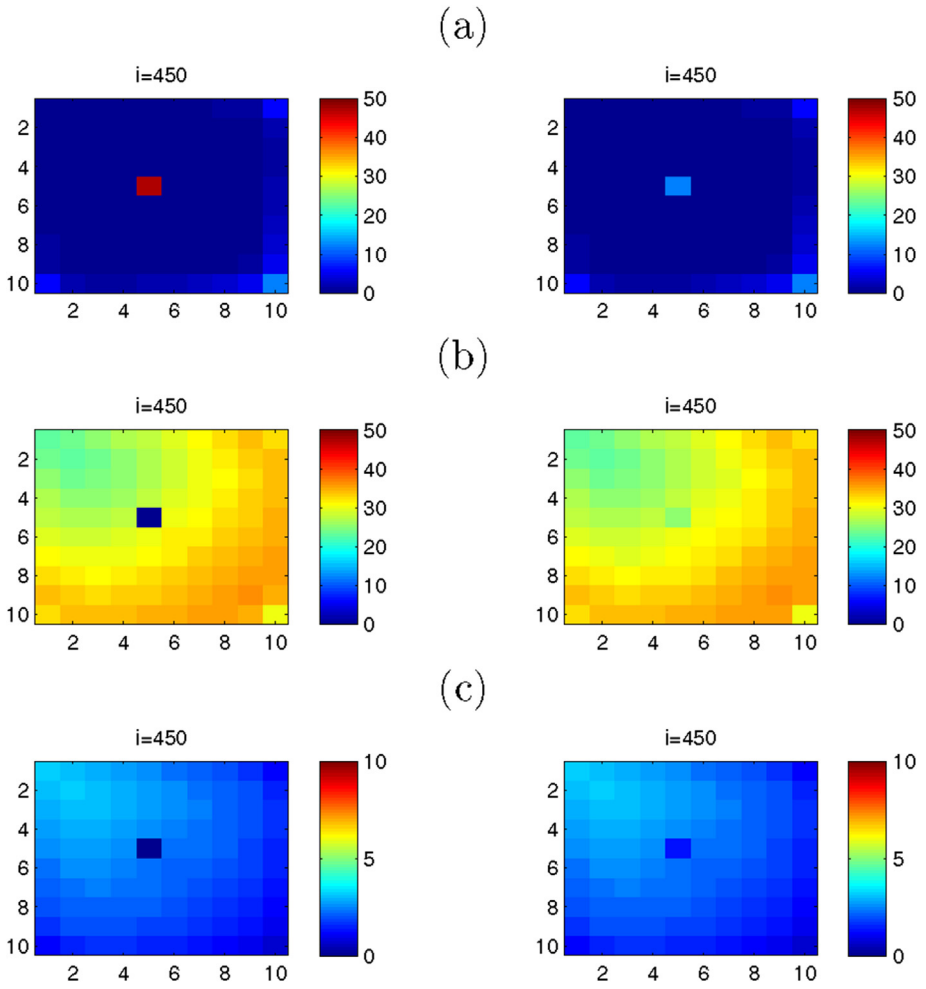

Fig. 17. SIR dynamics in Ω when the movements of $I^{C_{rs}}$ are restricted $\forall C_{rs} \in V_{pq}$, and when $C_{rs} \in V_{pq} \setminus C_{45}$. (a): $S^{C_{pq}}$ behavior. (b): $I^{C_{pq}}$ behavior. (c): $R^{C_{pq}}$ behavior.

infection starts from C_{65} with 10 individuals at $i = 0$, and then, the maximum value can not be the same as in other cells since that leads to a bigger value of dead people in C_{65} than any other cell, and this can also be observed at the final instant, where $I^{C_{65}}$ decreases to 7 individuals while it decreases to the same number plus one in other cells.

Fig. 16 illustrates shapes of the optimal controls which restrict movements of infected people coming from V_{55}, taking 0.925×10^{-3} as maximal value in all cells, except in the cell C_{65} where $I^{C_{65}}$ increases towards the same value but minus 0.025×10^{-3}. The values of the optimal controls are small but realizes our main objective presented in (7), but the most important idea we can extract from results in both Figs. 15 and 16, is that there is an analogy between shapes of infection and optimal controls functions since whenever the infection is maximal, the optimal controls which is associated with it, becomes simultaneously maximal. Respectively, this remains true when the infection is minimal as we can see at final times. In fact, even at initial conditions there is an analogy between $u^{55C_{rs}}$ and $I^{C_{rs}}$ as we can see for instance, in simulations of $u^{55C_{65}}$ and $I^{C_{65}}$. This also means that once an infection is detected in the vicinity of the targeted cell, the travel-blocking optimal controls function, responds automatically at the same time.

In Fig. 17, we choose to investigate behaviors of the $S^{C_{pq}}$, $I^{C_{pq}}$ and $I^{C_{pq}}$ functions when we do not follow the travel-blocking vicinity optimal control approach in only one cell from V_{55}. The cellular simulations at the left side, illustrate the SIR dynamics of the case studied in Figs. 8–13, while numerical results at the right side, depict the same behaviors but in the particular case when we do not restrict movements of infected individuals which come from cell C_{45}. In (a), we can see when we have realized that $S^{C_{55}}_{450}$ has not changed significantly regards to $S^{C_{55}}_{0}$, it loses now more people as seen in the cellular simulations at the right side, since the infection which enters from C_{45}, has proved to be sufficient to change $S^{C_{55}}_{450}$ from 45 to only 15 individuals. This can be more understood from (c), where we can observe that $I^{C_{55}}_{450}$ has increased from zero value in the case of a total travel-blocking strategy which concerns all cells of V_{55}, to 25 individuals in this new case. Simultaneously, when $S^{C_{55}}_{450}$ increases, $R^{C_{55}}_{450}$ in (c), decreases to 2 individuals, instead of no removed people at the left side because the number of infected people in C_{55} has been insignificant in that case, and then no one could move to the recovery state. This kind of comparisons allows us to show the reason behind proposing in this paper, such kind of optimal control strategies applied to all cells which belong to the vicinity of a cell we aim to control.

5. Conclusion

Some researchers have exploited the framework of compartmental modeling in epidemiology and tried to introduce the concept of networks-based models either for the description of some phenomena that take place within complex social, economic, and technological systems. (Barrat, Barthelemy, & Vespignani, 2008; Easley & Kleinberg, 2010; Newman, 2010, pp. 1–2) and references therein.

In this paper, we devised a multi-regions discrete-time model which describes infection dynamics due to the presence of an epidemic in one region and which spreads to other regions via travel. Regions have been assembled in one grid of cells where each cell represents a region, in order to exhibit the impact of infection which comes from the vicinity of a cell. In fact, by this kind of representations, we have succeeded to show the effectiveness of the travel-blocking vicinity optimal control approach when it is applied to only one cell, and then, we demonstrated that when we restrict movements of infected people coming from the vicinity of one targeted cell, we can keep this cell safe, and without/or with no important infection.

These modeling and optimal control approaches have also led us to three major results:

- When an epidemic starts near the center of a global domain of interest, the situation becomes more severe in terms of the number of infected individuals compared to the case when the epidemic starts from a corner. This is due to the number of cells in the vicinity of the cell that represents the source of infection.
- The optimal controls introduced in our mathematical model, respond automatically to the epidemic once it is detected, and there is an analogy between their shapes and the shape of infection.
- If we do not apply the travel-blocking vicinity optimal control strategy to only one cell from the vicinity of the targeted cell, the other optimal controls are not sufficient to stop/or to reduce the infection in the controlled cell.

The cellular simulations we presented in the numerical results section, have illustrated the case of 100 cells threatened by infection coming from one cell located once in the corner of a global domain of interest, and an other time near the center of this domain, while the targeted cell aiming to control, was chosen exactly in the center.

Acknowledgement

We would like to thank all members of the editorial board and referees for their valuable comments.

This work is supported by the Systems Theory Network (Réseau Théorie des Systèmes), and Hassan II Academy of Sciences and Technologies-Morocco.

References

Afia, N., Singh, Manmohan, & Lucy, David (2014). Numerical study of SARS epidemic model with the inclusion of diffusion in the system. *Applied Mathematics and Computation, 229*, 480–498 (2014).

Barrat, A., Barthelemy, M., & Vespignani, A. (2008). *Dynamical processes on complex networks*. Cambridge University Press.

Chunxiao, D., Tao, N., & Zhu, Y. (2016). A mathematical model of Zika virus and its optimal control. In *Control conference (CCC), 2016 35th Chinese* (pp. 2642–2645). TCCT.

Dabbs, K. (2010). *Optimal control in discrete pest control models*. Thesis http://trace.tennessee.edu.

Easley, D., & Kleinberg, J. (2010). *Networks, crowds, and markets: Reasoning about a highly connected world*. Cambridge University Press.

Fray, M. D., Paton, D. J., & Alenius, S. (2000). The effects of bovine viral diarrhoea virus on cattle reproduction in relation to disease control. *Animal Reproduction Science, 60*, 615–627.

Grubman, M. J., & Baxt, B. (2004). Foot-and-mouth disease. *Clinical Microbiology Reviews, 17*(2), 465–493.

Kermack, W. O., & McKendrick, G. A. (1927). A contribution to the mathematical theory of epidemics. *Proceedings of the Royal Society of London A: Mathematical, Physical And Engineering Sciences, 115*(772), 700–721. The Royal Society.

Newman, M. (2010). *Networks: An introduction*. New York: United Slates: Oxford University Press Inc.

Samanta, G. P. (2011). Permanence and extinction of a nonautonomous HIV/AIDS epidemic model with distributed time delay. *Nonlinear Analysis: Real World Applications, 12*(2), 1163–1177.

Sánchez-Vizcaíno, J. M., Mur, L., & Martínez-López, B. (2012). African swine fever: An epidemiological update. *Transboundary and Emerging Diseases, 59*(s1), 27–35.

Sethi, S. P., & Thompson, G. L. (2000). *What is optimal control theory?* US: Springer.

Thiaucourt, F., Yaya, A., Wesonga, H., Huebschle, O. J. B., Tulasne, J. J., & Provost, A. (2000). Contagious bovine pleuropneumonia: A reassessment of the efficacy of vaccines used in Africa. *Annals of the New York Academy of Sciences, 916*(1), 71–80.

Wandi, D., Hendon, R., Cathey, B., Lancaster, E., & Germick, R. (2014). Discrete time optimal control applied to pest control problems. *Involve, a Journal of Mathematics, 7*(4), 479–489.

Zakary, O., Larrache, A., Rachik, M., & Elmouki, I. (2016). Effect of awareness programs and travel-blocking operations in the control of HIV/AIDS outbreaks: A multi-domains SIR model. *Advances in Difference Equations, 2016*(1), 1–17.

Zakary, O., Rachik, M., & Elmouki, I. (2016a). On the analysis of a multi-regions discrete SIR epidemic model: An optimal control approach. *International Journal of Dynamics and Control*, 1–14.

Zakary, O., Rachik, M., & Elmouki, I. (2016b). A new analysis of infection dynamics: Multi-regions discrete epidemic model with an extended optimal control approach. *International Journal of Dynamics and Control*, 1–10.

Zakary, O., Rachik, M., & Elmouki, I. (2016c). A multi-regional epidemic model for controlling the spread of Ebola: Awareness, treatment, and travel-blocking optimal control approaches. *Mathematical Methods in the Applied Sciences*.

Zakary, O., Rachik, M., & Elmouki, I. (2016d). On the impact of awareness programs in HIV/AIDS prevention: An SIR model with optimal control. *International Journal of Computer Applications, 133*(9), 1–6.